NANO LETTERS

Letter

pubs.acs.org/NanoLett

Highly Responsive Ultrathin GaS Nanosheet Photodetectors on Rigid and Flexible Substrates

PingAn Hu,*[,†] Lifeng Wang,[†] Mina Yoon,[‡] Jia Zhang,[†] Wei Feng,[†] Xiaona Wang,[†] Zhenzhong Wen,[†] Juan Carlos Idrobo,[§] Yoshiyuki Miyamoto,[∥] David B. Geohegan,[‡] and Kai Xiao*[,‡]

[†]Key Lab of Microsystem and Microstructure, Harbin Institute of Technology, Ministry of Education, No. 2 YiKuang Street, Harbin, 150080, P. R. China

[‡]Center for Nanophase Materials Sciences and [§]Materials Science and Technology Division, Oak Ridge National Laboratory, One Bethel Valley Road, Oak Ridge, Tennessee 37831, United States

[∥]Nanosystem Research Institute, National Institute of Advanced Industrial Science and Technology (AIST), Central 2, 1-1-1 Umezono, Tsukuba 305-8568, Japan

Supporting Information

ABSTRACT: The first GaS nanosheet-based photodetectors are demonstrated on both mechanically rigid and flexible substrates. Highly crystalline, exfoliated GaS nanosheets are promising for optoelectronics due to strong absorption in the UV−visible wavelength region. Photocurrent measurements of GaS nanosheet photodetectors made on SiO_2/Si substrates and flexible polyethylene terephthalate (PET) substrates exhibit a photoresponsivity at 254 nm up to 4.2 AW^{-1} and 19.2 AW^{-1}, respectively, which exceeds that of graphene, MoS_2, or other 2D material-based devices. Additionally, the linear dynamic range of the devices on SiO_2/Si and PET substrates are 97.7 dB and 78.73 dB, respectively. Both surpass that of currently exploited InGaAs photodetectors (66 dB). Theoretical modeling of the electronic structures indicates that the reduction of the effective mass at the valence band maximum (VBM) with decreasing sheet thickness enhances the carrier mobility of the GaS nanosheets, contributing to the high photocurrents. Double-peak VBMs are theoretically predicted for ultrathin GaS nanosheets (thickness less than five monolayers), which is found to promote photon absorption. These theoretical and experimental results show that GaS nanosheets are promising materials for high-performance photodetectors on both conventional silicon and flexible substrates.

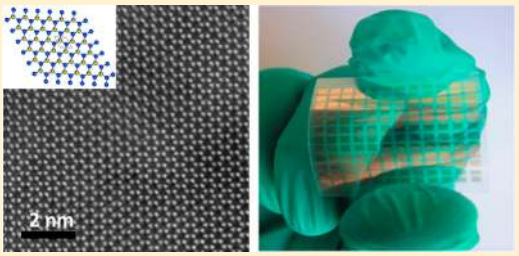

KEYWORDS: *Gallium sulfide, two-dimensional materials, nanosheets, photodetectors, photoresponsivity*

Ultrathin two-dimensional (2D) nanomaterials are a highly promising new class of materials that are revealing exotic properties with great promise for application in next generation electronics and optoelectronic devices. Compared to quantum dots and one-dimensional materials such as semiconductor nanowires and carbon nanotubes, 2D materials are more compatible with current thin film micromanufacturing techniques and are more easily fabricated into complex structures. Graphene is the most widely studied 2D nanomaterial so far because of its unusual electrical, optical, magnetic, and mechanical properties.[1−5] Graphene is particularly promising for wideband, high speed photodetectors due to its wide band absorption, high carrier mobility, and short carrier lifetime.[6] For example, graphene-based photodetectors have been demonstrated with ultrahigh operation frequencies comparable to or even exceeding traditional group III−V semiconductor-based photodetectors.[7] Graphene photodetectors have also been exploited for ultrawide band (300 nm ∼ 6 μm) operation, far exceeding the performance of current photodetectors.[8,9] However, several problems remain with graphene photodetectors, notably their low responsivity (∼10^{-2} AW^{-1}), very low external quantum efficiency (QE) (0.1−0.2%),[10] and absence of spectral selectivity. Graphene's low photoresponse and low external quantum efficiency are caused by weak light absorption and fast recombination of photoinduced carriers.[10] The absence of spectral selectivity in graphene photodetectors originates from the wavelength-independent absorption characteristics of graphene due to the constant universal conductivity for Dirac fermions.[6] Subsequently, considerable efforts have been made to improve the light absorption by exploring the thermoelectric, plasmonic, or microcavity effects of graphene.[11−14] In addition, since quantum dot-based photodetectors have exhibited large photoconductive gains with spectacular responsivity (10^3 AW^{-1}), hybrid graphene-quantum dot systems have been constructed to increase the light absorption and spectral selectivity of graphene photodetectors.[15] But these methods increase fabrication complexity. Therefore, extensive research

Received: January 10, 2013
Revised: February 28, 2013
Published: March 6, 2013

efforts are being performed to investigate semiconducting 2D nanostructures of elements other than carbon for device applications.

It is well-known that the large surface-to-volume ratio and the lower dimensionality of nanostructured materials can yield higher light sensitivity than their bulk counterparts and that the photocarrier lifetime is considerably prolonged due to charge separation promoted by surface states.[16−18] Compared to graphene-based devices, photodetectors made from inorganic semiconducting ultrathin nanosheets, analogues to graphene, could show enhanced responsivity and spectral selectivity. Recently, significant progress has been demonstrated in semiconducting ultrathin nanosheet-based electronics and optoelectronics.[19−22] The mobility of a single-layer MoS_2 transistor was improved to ~200 cm^2 V^{-1} s^{-1} by using a high *k* dielectric layer of hafnium oxide.[19] A single-layer MoS_2-based photodetector was recently demonstrated with an improved spectral responsivity of 7.5 mAW^{-1} compared to similar graphene-based photodetectors (~1 mAW^{-1}).[20] A p-type FET with room-temperature hole mobility of 250 cm^2 V^{-1} s^{-1} was recently demonstrated using an active channel made of single-layer WSe_2.[21] Recently, we fabricated few-layer GaSe nanosheet UV photodetectors exhibiting a responsivity of 2.8 AW^{-1}, which is orders of magnitude higher than the similar devices made from pristine graphene or single-layer MoS_2.[22]

GaS belongs to III−VI group of layered compounds with each layer consisting of S−Ga−Ga−S repeating units stacked along *c*-axis. Interlayer interactions are dominated by the weak van der Waals force, while interlayer-bonding forces are covalent in nature. GaS is considered as a promising material for near-blue light emitting devices because it has an indirect band gap at 2.59 eV at 300 K and a direct band gap at approximately 3.05 eV,[23] Crystalline single-layer or few-layer GaS nanosheets can be efficiently obtained using a mechanical cleavage approach, and subsequently transferring to SiO_2/Si wafer and other substrates.[24] Some investigations have performed on optoelectronic properties of single crystal and amorphous GaS, both showing high yield optoelectronic conversion in the red and blue visible regions.[25,26] 1D GaS nanowires and nanobelts have been synthesized using a vapor−solid method and exhibited strong photoluminescence and field-emission behavior.[27,28] Ultrathin GaS bottom-gate transistors with mobilities of 0.1 cm^2 V^{-1} s^{-1} have been demonstrated by Dravid et al.[29] However, comparable ultrathin GaS-based photodetectors have not been previously reported. Flexible devices, which exploit bendable plastic substrates, are emerging as promising next-generation candidates for electronics,[30] optoelectronic applications,[31,32] as well as chemical sensors.[33] It is important to explore the suitability of easily exfoliated, new 2D-nanosheet such as GaS on flexible plastics for applications such as photodetectors and other devices.

Here, the first GaS nanosheet photodetectors are reported on both rigid substrate (SiO_2/Si) and flexible plastics (polyethylene terephthalate PET) substrates. The photodetectors exhibit high photoresponsivities, increasing in the ultraviolet to 19.2 AW^{-1} with external quantum yields up to 9374% at 254 nm, which are much higher than those of pristine graphene photodetectors (1×10^{-3} AW^{-1}, 6−16%).[10] Theoretical modeling of the GaS nanosheet electronic structures indicates that the reduction of the effective mass at the valence band maximum (VBM) with decreasing sheet thickness enhances the carrier mobility of the GaS nanosheets, contributing to the high photocurrents. Double-peak valence band maxima are theoretically predicted for ultrathin GaS nanosheets (less than five monolayers) which are found to promote photon absorption.

Ultrathin GaS nanosheets were characterized by scanning electron microscopy (SEM), atomic force microscopy (AFM), transmission electron microscopy (TEM), and Raman spectroscopy. Figure 1a presents the crystal structure of monolayer

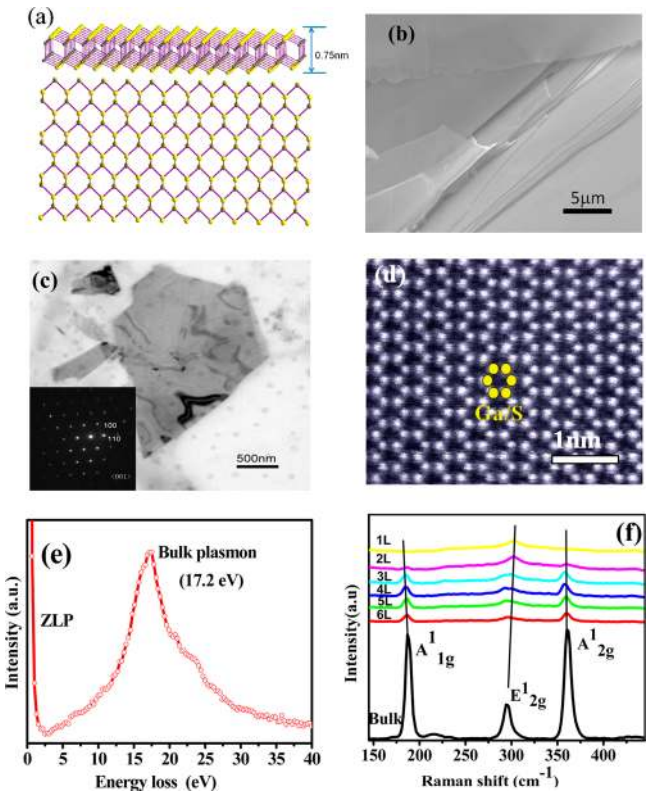

Figure 1. Characterization of GaS nanosheets: (a) scheme of crystal structure: monolayer GaS with a thickness of 0.75 nm and (001) plane of monolayer GaS (bottom); (b) a typical SEM image of GaS nanosheets; (c) a typical low-resolution TEM image of GaS nanosheets; the inset is the selected area diffraction pattern of GaS nanosheets; (d) *Z*-contrast STEM image showing the atomic structure of the GaS nanoflake; (e) valence EEL spectra of a GaS nanoflake. For this particular nanosheet, the bulk plasmon was located at 17.2 eV. (f) Raman spectra of bulk GaS and GaS nanosheet with different layer numbers.

GaS sheet with a thickness of 0.75 nm. Bottom Figure 1a shows a top view of monolayer GaS crystal structure consisting of six-atom hexagonal rings. Figure 1b shows a typical SEM image of GaS nanosheet, presenting clear layer-like sheets. Figure 1c gives a typical TEM image, and the selected area (2 μm × 2 μm) electron diffraction pattern (inset) indicates that the GaS nanosheet is formed by single crystals. A high-resolution scanning transmission electron microscopy (STEM) image shown in Figure 1d indicates that the (001) plane of GaS nanosheet is composed of six-atoms forming a hexagonal ring, which corresponds well with the simulated structure of (001) plane. Electron energy loss spectroscopy (EELS) obtained from the sample (Figure 1e) indicates that the bulk plasmon of the thin flakes is located at 17.2 eV. To further characterize the flakes, their chemical compositions were measured by energy-dispersive X-ray spectroscopy (EDS) (Figure S1), confirming that the nanosheets have a Ga/S stoichiometric ratio of ~1:1. The thickness of the as-prepared GaS sheets was measured by

dx.doi.org/10.1021/nl400107k | *Nano Lett.* 2013, 13, 1649−1654

AFM to be within the range of ~0.8−5 nm (monolayer GaS shown in Figure S2).

Raman spectroscopy is a convenient tool for nondestructive characterization and identification of ultrathin layer materials. Figure 1f shows the comparative Raman spectra of bulk and ultrathin layers of GaS. Bulk GaS shows Raman modes E^1_{1g} (72 cm^{-1}), A^1_{1g} (187.3 cm^{-1}), E^1_{2g} (294.1 cm^{-1}), and A^1_{2g} (360.2 cm^{-1}). In the GaS monolayer, the shifts of Raman modes at room temperature are E^1_{1g} (75.2 cm^{-1}), E^1_{2g} (303.5 cm^{-1}), and the Raman vibrations at A^1_{1g} and A^2_{1g} are so weak that their peaks are invisible. As the number of layers (L) increases from 1 to 6 L, the frequency of the E^1_{2g} mode decreases and that of A^1_{1g} and A^1_{2g} mode increases, which corresponds well with the reported Raman spectrum in the thin exfoliated GaS film[24] since the sign of the shift of the E^1_{2g} mode is unexpected within models of weak van der Waals interlayer coupling. This shift suggests a role for stacking-induced changes in intralayer bonding and/or the presence of Coulombic interlayer interactions in GaS, which has also been observed in GaSe and MoS_2.[22,23]

To measure the photoresponse behavior of ultrathin GaS nanosheets devices on the SiO_2/Si substrate, monochromatic light illumination was directed vertically onto the device consisting of two Cr/Au electrodes and a 20 μm length channel, with a 10 μm wide GaS nanosheet on a Si substrate with 300 nm SiO_2 insulating top layer (depicted in Figure 2a with the inset image showing a typical device). The thickness of the GaS nanosheets in this device is ~3 layers as estimated by Raman spectroscopy measurements. The corresponding photocurrent behavior is recorded (shown in Figure 2). Figure 2b shows photocurrent as a function of applied bias voltage (V_{DS}) when GaS nanosheet photodetectors were illuminated with different wavelengths with irradiance of 0.5 mW/cm^2 and under dark conditions. The wavelength-dependent photocurrent response in Figure 2c shows that there is almost a 10^4 times increase in the photocurrent at 254 nm compared to at 610 nm, indicating that 2D GaS based photodetectors are highly spectrally selective to UV−visible light, the response doubling at 254 nm compared to 365 nm. This characteristic spectral selectivity originates from the bandgap inherent in the band structure of the GaS nanosheets, in contrast to graphene with zero bandgap. In GaS nanosheets, photons with energy higher than the bandgap of 2D GaS (~3.05 eV, wavelength <520 nm) can produce hole−electron pairs. Higher photon energies provide higher excitation energy which are found to increase the photocurrent. As shown in Figure 2d, with the light irradiation at 254 nm on and off, the current in the devices showed a "low" dark current of ~1.36×10^{-4} nA and a "high" current of 4 nA, giving an high on/off switching ratio of 2.94×10^4, proving that the GaS nanosheet photodetector is highly responsive. The switching between these two states is very fast and reversible, allowing the device to act as a high quality photosensitive switch. The response time is faster than the detection limit of the measurement setup (30 ms), which is already faster than single-layer MoS_2 devices (response time: 50 ms).[22] The high photocurrent was confirmed at different light intensities (as shown in Figure 2e). The photocurrent shows a strong dependence on light intensity and displays a power dependence of ~1.17 (function: $I_{ph} = 7.618P^{1.17}$), indicating a superior photocurrent capability of the 2D GaS nanosheets. In addition, we found out that the photocurrent of the GaS device was almost invariant during irradiation times <30 min but significantly decreases during long-term operation (~40% decrease after 2 h, Figure S3), most likely due to oxidation induced by deep-UV irradiation in air.

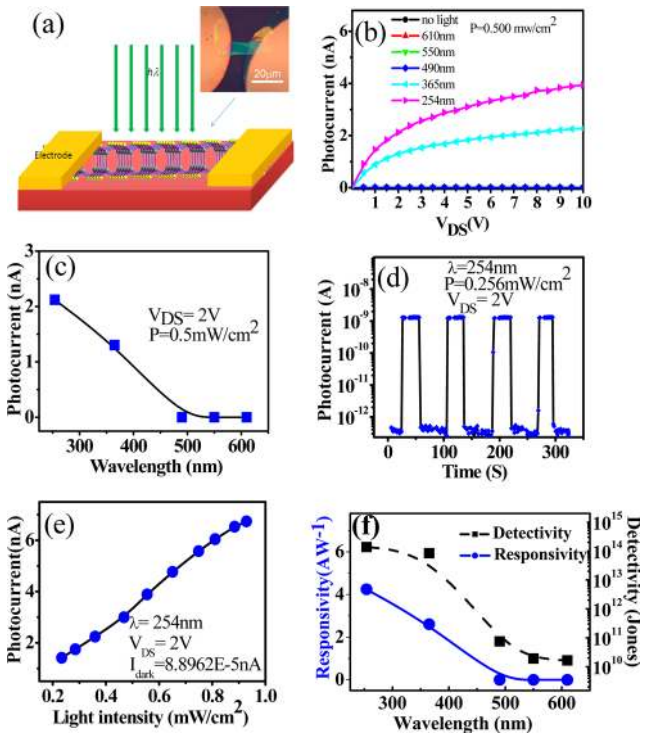

Figure 2. GaS nanosheet photodetector on SiO_2/Si substrate: (a) Schematic of the device structure (inset: optical image of an actual device); (b) $I-V$ curves of photodetectors illuminated with different wavelengths; (c) wavelength dependent photocurrent; (d) photocurrent as function of time under pulse illumination at bias voltage of 2 V; (e) photocurrent as function of illumination density, LDR of the device under light irradiation of 254 nm. The inset is the dark current of the device, V_{DS} = 2 V; (f) wavelength-dependent photoresponsivity and photodetectivity.

Critical parameters for a photodetector are the detector current responsivity (R_λ), defined as the photocurrent generated per unit power of the incident light on the effective area of a photoconductor, and the external quantum efficiency (EQE) defined as the number of photoinduced carrier detected per incident photons. R_λ and EQE can be calculated by $R_\lambda = \Delta I/PS$ and EQE = $hcR_\lambda/e\lambda$, where ΔI is the photoexcited current; P is the light power intensity irradiated on the GaS nanosheet; S is the effective area of photodetector; h is Planck's constant; e is electron charge; and λ is the excitation wavelength.[22] From our experimental results, under an illumination of 254 nm at 2 V, the R_λ and EQE are calculated to be ~4.2 AW^{-1} and ~2050%, respectively. These performance data are about 1000 times higher than photodetectors reported for graphene or single-layer MoS_2.[20] Moreover, the GaS nanosheet photodetector shows a wavelength dependent responsivity as shown in Figure 2f, in which R_λ are estimated to be 5.06×10^{-4} AW^{-1} for 610 nm, 7.74×10^{-4} AW^{-1} for 550 nm, 2.3×10^{-3} AW^{-1} for 490 nm, 2.60 AW^{-1} for 365 nm, and 4.24 AW^{-1} for 254 nm using a fixed illumination power of 0.5 mW/cm^2. This wavelength-dependent responsivity corresponds well with the fact that higher excitation energy enhances the conversion of photoelectronics.

Another important parameter to quantify the photodetector sensitivity is the detectivity (D^*), which measured in units of

dx.doi.org/10.1021/nl400107k | Nano Lett. 2013, 13, 1649−1654

Jones. Since the shot noise from the dark current is the major contribution to the total noise in our case, the detectivity can be given by $D^* = RA^{1/2}/(2eI_d)^{1/2}$, where R is the responsivity, A is the effective area of the detector, e is the absolute value of electron charge, and I_d is the dark current density.[34] Figure 2f shows the calculated D^* of the GaS nanosheet photodetector on SiO_2/Si at different wavelengths. For the visible region of the spectrum, D^* is in the range of $\sim 10^{10}$ Jones, and for ultraviolet light, D^* is in the range of $\sim 10^{13}-10^{14}$ Jones, which is comparable to the performance of silicon photodiodes ($D^* \sim 10^{13}$ Jones).[34]

To measure the performances of GaS nanosheet photodetectors on flexible plastic substrates, exfoliated GaS nanosheets were transferred onto PET substrates and were subsequently patterned with Au electrode contacts using a shadow mask. Figure 3a shows a typical optical image of wafer-scale GaS nanosheet devices on PET. Figure 3b shows a typical magnified image of an individual device with an electrode channel of 15 μm. The photocurrent generated is highly linear with the light intensity as shown in Figure 3c, indicating good photoresponse for GaS nanosheet photodetectors on plastic substrates. Figure 3d shows the calculated responsivity (R_λ) and detectivity (D^*) at different wavelengths under a fixed irradiance of 0.5 mW/cm^2. R_λ are calculated to be 0.95 AW^{-1} for 550 nm, 1.56 AW^{-1} for 490 nm, 15.3 AW^{-1} for 365 nm, and 19.2 AW^{-1} for 254 nm. D^* is in the range of $10^{12}-10^{13}$ Jones for visible light and about 10^{14} Jones for ultraviolet light, which surpass the detectivity of existing InGaAs devices ($D^* \sim 10^{12}$ Jones). Compared to the devices on SiO_2/Si, the GaS nanosheet photodetectors on flexible PET substrates display a higher photoresponse. For example, the flexible GaS nanosheet device shows a photoresponsivity of 19.2 AW^{-1} under the irradiation of 254 nm, which is almost four times as large as that for the device on SiO_2/Si (4.24 AW^{-1}). This performance difference is possibly due to the existence of hydroxyl groups or other structural defects at the SiO_2 interface which can trap photoexicited charges and impede the photocurrent in GaS. Further investigations will be performed to understand how the intrinsic nature of the substrate influences the photoresponse of GaS nanosheets.

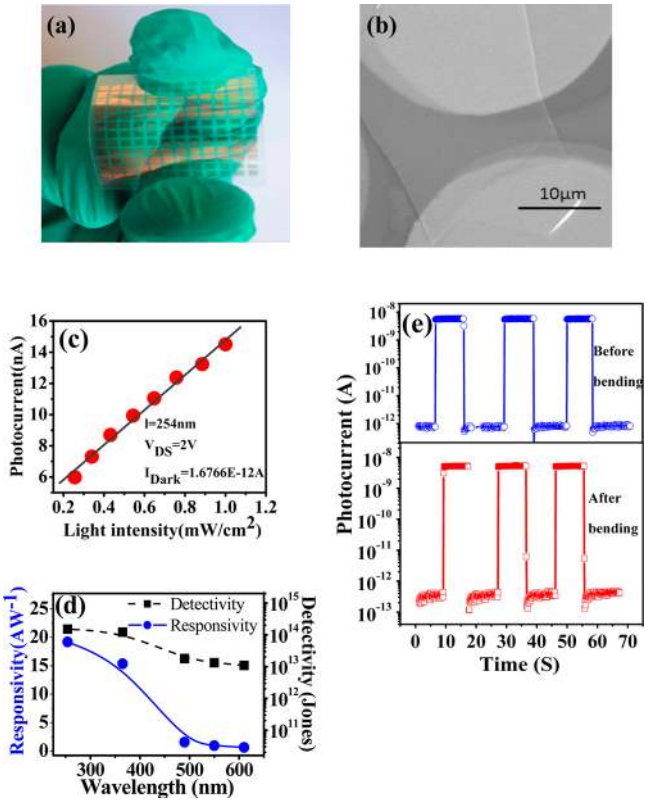

Figure 3. GaS nanosheet photodetector on PET substrate: (a) optical image of GaS nanosheet devices on PET substrate; (b) a SEM image of single device; (c) photocurrent as function of illumination density, LDR of the device under light irradiation of 254 nm. Inset is the dark current of the device. V_{DS} = 2 V; (d) wavelength-dependent photoresponsivity and photodetectivity under 0.5 mW/cm^2 irradiance at a bias voltage of 2 V; (e) photocurrent as function of time before or after bending with the pulse illumination at bias voltage of 2 V.

Flexible optoelectronics are easily subjected to a variety of mechanical deformations that may degrade their performance, including bending, compression, and tension. To investigate the stability of the GaS nanosheet devices after flexure, the photoresponse of the devices on PET substrates was measured before/after bending. Figure 3e plots the photoresponse versus time characteristics of the photodetectors exposed to pulsed light illumination after bending the substrate 20 times to an angle of 60°. The photoresponse rise and fall times of $\lesssim$ 30 ms and the high on/off switching ratio of $\sim 1.5 \times 10^4$ is invariant of bending, indicating that GaS nanosheet photodetectors on PET substrates are highly responsive and stable, which is of paramount significance to the future 2D semiconductor nanostructure-based optoelectronics. Further, the performances of the devices have been measured during bending at different angles (Figure S4). The photocurrent and responsivity of the GaS photodetectors decline a factor of 2 upon bending to 60°, in agreement with the factor of 2 decrease in effective irradiance.

An important photodetector parameter is the linear dynamic range (LDR), or the photosensitivity linearity (typically quoted in dB). The LDR is given by LDR = 20 log(I_{ph}/I_{dark}), where I_{ph} is the photocurrent, measured at light intensity of 1 mW cm^{-2}. The LDR was calculated from Figures 2f and 3d under illumination with visible light from a 500 W halogen lamp. The calculated LDR of the GaS nanosheet device on SiO_2/Si and PET substrates are 97.7 dB and 78.73 dB, respectively. Both values exceed that of currently used InGaAs photodetectors (66 dB),[35] indicating that GaS nanosheet devices are highly promising next generation photodetectors.

The performance parameters of the GaS nanosheet photodetectors are compared in Table 1 to other reported 2D nanosheet optical devices. GaS nanosheet photodetectors show

Table 1. Comparison of the Critical Parameters for the Reported 2D-Nanostructure Photodetectors

photodetectors	responsivity (R_λ) [AW^{-1}]	quantum efficiency (QE) [%]	response time	reference
graphene (on SiO_2/Si)	1×10^{-3}	6–16	~ps	7
single layer MoS_2 (on SiO_2/Si)	7.5×10^{-3}		50 ms	20
few-layer GaSe (on SiO_2/Si)	2.8	1367	20 ms	22
GaS nanosheet (on SiO_2/Si)	4.2	2050	<30 ms	this work
GaS nanosheet (on PET)	19.2	9371	<30 ms	this work

dx.doi.org/10.1021/nl400107k | Nano Lett. 2013, 13, 1649–1654

a higher responsivity and external quantum efficiency than several other reported 2D nanosheet devices[7,20,22] and a faster response time than single-layer MoS_2 photodetectors.[20] These performance parameters are comparable with similar devices made of nanowires, nanotubes, and quantum dots.[15,35,36] Although some nanoscale photodetectors have been demonstrated with nanowires or nanotubes in the past 10 years,[37,38] their practical application in high yield, scalable systems faces formidable engineering challenges in assembly as well as other aspects of manufacturing. 2D materials can avoid these limitations since they are compatible with established device designs and processing approaches in the semiconductor industry. All of these results indicate that GaS nanosheets are promising for highly sensitive nanoscale photodetectors.

To understand the origin of the observed enhancement in the photocurrent of the GaS nanosheets, electronic structure calculations were performed using a highly accurate, all-electron first-principles quantum mechanical calculation code (FHI-aims).[39] The exchange-correlation potential of the Perdew–Burke–Ernzerhof (PBE) version of the generalized-gradient approximation (GGA) was used.[40,41] The experimentally observed nanosheets were theoretically modeled as a slab consisting of a pair of GaS monolayers in a supercell, where the atomic arrangement of in-planar layer directions (x and y directions) are infinitely repeating and the layer stacked direction (z-direction) has a sufficiently large empty space ("vacuum" of ~50 Å) to avoid any artificial interactions between the neighboring cells in the z-direction. For k-point samplings, 11 × 11 × 6 mesh points were used for bulk and 11 × 11 × 1 for the nanosheets with a large size vacuum (~50 Å). The atomic coordinates of β-GaS phase were used for these calculations with lattice constants, a = 3.585 Å and c = 15.5 Å for bulk simulation (which consisted of two layers), and for slabs a = 3.585 Å and c = 7.75 Å multiplied by the number of monolayers in the slab.

Figure 4a shows the electronic band structures of monolayer (ML) GaS and the GaS bulk phase using the PBE functional,

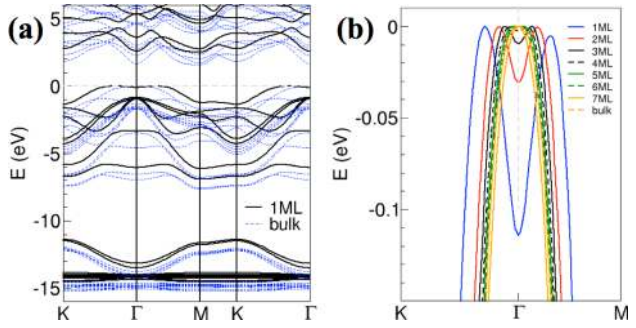

Figure 4. (a) Electronic band structures of 1 ML GaS compared with its bulk phase using PBE functional. Here the energy level is plotted with respect to the valence band maximum, and the horizontal dotted line is for guidance for the zero line. (b) The valence bands are redrawn to emphasize the effective masses and double valence band maximum features for up to 4 ML nanosheets.

where the energy reference is the valence band maximum (VBM). The location of the VBM is at the Γ point for the bulk, whereas the conduction band minimum (CBM) is located at M. The predicated indirect band gap of bulk GaS is 1.59 eV. For the 1 ML nanosheet, the indirect band gap is significantly higher (2.50 eV). Moreover, the location of the VBM is slightly shifted in a symmetric way with respect to the Γ point, which results in a double-peak VBM with a slight valley located at Γ. As shown in Figure 4b, which magnifies the band structures near the VBM, this double-peak VBM feature is predicted only for nanosheets ≤4 ML thickness. For all thicker nanosheets, their VBM are at Γ.

As shown in Figure 5a the band gap energy significantly increases as the nanosheets become thinner, converging to

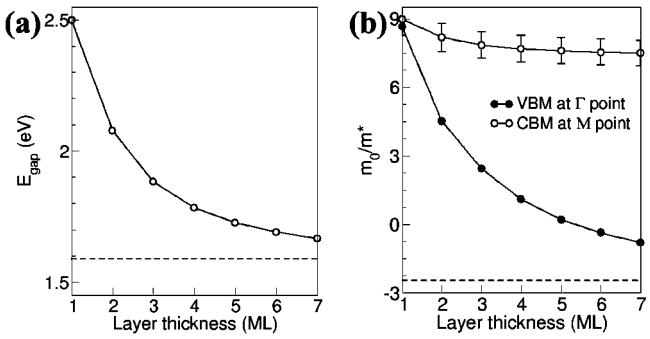

Figure 5. (a) Energy band gap of GaS nanosheets as a function of layer thickness (number of monolayers, ML) using the PBE functional within the *ab initio* density functional theory; (b) Inverse of the effective masses (m^*) of electrons for the valence band maximum (VBM) at the Γ point and conduction band minimum at the M point, with respected to the free electron mass, m_0. Those values are obtained by interpolating the VBM (CBM) at Γ (M) from the band structure calculations, and the error bars from the fitting are also plotted as the vertical lines. For the VBM effective mass, the error is too small to be visible.

within less than ~0.1 eV after the thickness reaches ~6 ML. The absolute values of the predicated bandgaps are much smaller than the experimental values, as could be expected from the semilocal exchange-correlation functionals. The issues with the accuracy of the functionals can be found elsewhere. The effective mass (m^*) of the charge carriers was calculated by interpolating the valence band at Γ and the conduction band at M. The inverse values of the effective masses are presented in Figure 5b with respect to the free electron mass m_0. It very interesting that the effective mass at the VBM significantly decreases as the layer number decreases, while no significant changes are predicated for the CBM effective mass. The reduction of the effective mass enhances carrier mobility of the GaS nanosheets, resulting in high photocurrent. In addition, the double peak feature in the VBMs for the nanosheets of thickness ≤4 ML (see Figure 4b) enhances the photoabsorption cross section since there are twice as many electrons available at the VBM in comparison to the single-peak VBM case. These theoretical calculations support the experimental observations of enhanced photocurrent and photoabsorption in GaS ultrathin nanosheets.

In conclusion, GaS nanosheet photodetectors on rigid (SiO_2/Si) and flexible (PET) substrates have been demonstrated for the first time. UV–visible photodetectors were made from ultrathin GaS nanosheets exfoliated from bulk crystals. The photoresponse and external quantum efficiency of the GaS nanosheet-based flexible photodetectors were measured at different wavelengths and reached 19.2 AW^{-1} and 9373%, respectively, at 254 nm. A theoretical investigation of the band structure in GaS nanosheets revealed two effects that may explain the origin of the enhanced photoresponse. For nanosheets less than 5 ML in thickness, a double peak in the valence band maximum emerged which could increase

dx.doi.org/10.1021/nl400107k | *Nano Lett.* 2013, 13, 1649–1654

photoabsorption by providing additional electron states. In addition, the effective electron mass was found to decrease with decreasing layer thickness, promoting higher photocurrents. These experimental and theoretical findings indicate that the two-dimensional nanostructure of GaS may be especially well suited for use in high performance nanoscale photodetectors.

■ ASSOCIATED CONTENT

Supporting Information

Experimental sections and instrumental information. This material is available free of charge via the Internet at http://pubs.acs.org.

■ AUTHOR INFORMATION

Corresponding Author

*E-mail: hupa@hit.edu.cn, xiaok@ornl.gov.

Notes

The authors declare no competing financial interest.

■ ACKNOWLEDGMENTS

This work is supported by the National Key Basic Research Program of China (973 Program) under Grant No. 2013CB632900, National Natural Science Foundation of China (NSFC, No. 61172001), the Scientific Research Foundation for the Returned Overseas Chinese Scholars, State Education Ministry and the Fundamental Research Funds for Central Universities and Chinese Program for New Century Excellent Talents in University. Part of research was conducted at the Center for Nanophase Materials Sciences (K.X., M.Y., D.B.G.) and ShaRE User Facility (J.C.I.), which are sponsored at Oak Ridge National Laboratory by the Scientific User Facilities Division, Office of Basic Energy Sciences, U.S. Department of Energy. M.Y. used resources of the National Energy Research Scientific Computing Center, which is supported by the Office of Science of the U.S. Department of Energy under Contract No. DE-AC02-05CH11231.

■ REFERENCES

(1) Geim, K.; Novoselov, K. S. *Nat. Mater.* **2007**, *6*, 183.
(2) Geim, K. *Science* **2009**, *324*, 1530.
(3) Rao, N. R.; Sood, A. K.; Subrahmanyam, K. S.; Govindaraj, A. *Angew. Chem., Int. Ed.* **2009**, *48*, 7752.
(4) Avouris, P.; Chen, Z.; Perebeinos, V. *Nat. Nanotechnol.* **2007**, *2*, 605.
(5) Schwierz, F. *Nat. Nanotechnol.* **2010**, *5*, 487.
(6) Nair, R. R.; Blake, P.; Grigorenko, A. N.; Novoselov, K. S.; Booth, T. J.; Stauber, T.; Peres, N. M. R.; Geim, A. K. *Science* **2008**, *320*, 1308−1308.
(7) Xia, F.; Mueller, T.; Lin, Y.; Valdes-Garcia, A.; Avouris, P. *Nat. Nanotechnol.* **2009**, *4*, 839−843.
(8) Zheng, J. P.; Jiao, K. L.; Shen, W. P.; Anderson, W. A.; Kwok, H. S. *Appl. Phys. Lett.* **1992**, *61*, 459−461.
(9) Khan, M. A.; Kuznia, J. N.; Olson, D. T.; Blasingame, M.; Bhattarai, A. R. *Appl. Phys. Lett.* **1993**, *63*, 2455−2456.
(10) Mueller, T.; Xia, F.; Avouris, P. *Nat. Photonics* **2010**, *4*, 297−301.
(11) Echtermeyer, T. J.; Britnell, L.; Jasnos, P. K.; Lombardo, A.; Gorbachev, R. V.; Grigorenko, A. N.; Geim, A. K.; Ferrari, A. C.; Novoselov, K. S. *Nat. Commun.* **2011**, *2*, 458.
(12) Koppens, F. H. L.; Chang, D. E.; Garcia de Abajo, F. J. *Nano Lett.* **2011**, *11*, 3370−3377.
(13) Thongrattanasiri, S.; Koppens, F. H. L.; Garcia de Abajo, F. J. *Phys. Rev. Lett.* **2012**, *108*, 047401.
(14) Furchi, M.; Urich, A.; Pospischil, A.; Lilley, G.; Unterrainer, K.; Detz, H.; Klang, P.; Andrews, A. M.; Schrenk, W.; Strasser, G.; Mueller, T. *Nano Lett.* **2012**, *12*, 2773−2777.
(15) Konstantatos, G.; Badioli, M.; Gaudreau, L.; Osmond, J.; Bernechea, M.; Pelayo Garcia de Arquer, F.; Gatti, F.; Koppens, F. H. L. *Nat. Nanotechnol.* **2012**, *7*, 363−368.
(16) Sun, Y. G.; Wang, H. H. *Adv. Mater.* **2008**, *19*, 2818.
(17) Li, L.; Fang, X. S.; Li, G. H. *J. Mater. Sci. Technol.* **2007**, *23*, 166.
(18) Li, L.; Koshizaki, N.; Li, G. H. *J. Mater. Sci. Technol.* **2008**, *24*, 550.
(19) Radisavljevic, B.; Radenovic, A.; Brivio1, J.; Giacometti1, V.; Kis, A. *Nat. Nanotechnol.* **2011**, *6*, 147−150.
(20) Yin, Z.; Li, H.; Jiang, L.; Shi, Y.; Sun, Y.; Lu, G.; Zhang, Q.; Chen, X.; Zhang, H. *ACS Nano* **2012**, *6*, 74−80.
(21) Fang, H.; Chuang, S.; Chang, T. C.; Takei, K.; Takahashi, T.; Javey, A. *Nano Lett.* **2012**, *12*, 3788−3792.
(22) Hu, P. A.; Wen, Z.; Wang, L.; Tan, P.; Xiao, K. *ACS Nano* **2012**, *6*, 5988−5994.
(23) Genut, M.; Margulis, L.; Hodes, G.; Tenne, R. *Thin Solid Films* **1992**, *217*, 97.
(24) Late, D. J.; Liu, B.; Matte, H. S. S. R.; Rao, C. N. R.; Dravid, V. P. *Adv. Funct. Mater.* **2012**, *22*, 1894.
(25) Ho, C. H.; Hsieh, M. H.; Wu, C. C. *Rev. Sci. Instrum.* **2006**, *77*, 113102.
(26) Aono, T.; Kase, K.; Kinoshita, A. *J. Appl. Phys.* **1993**, *74*, 2818.
(27) Shen, G. Z.; Chen, D.; Chen, P. C.; Zhou, C. W. *ACS Nano* **2009**, *3*, 1115.
(28) Sinha, G.; Panda, S. K.; Datta, A.; Chavan, P. G.; Shinde, D. R.; More, M. A.; Joag, D. S.; Patra, A. *ACS Appl. Mater. Interfaces* **2011**, *3*, 2130−2135.
(29) Late, D. J.; Liu, B.; Luo, J.; Yan, A.; Ramakrishna Matte, H. S. S.; Grayson, M.; Rao, C. N. R.; Dravid, V. P. *Adv. Mater.* **2012**, *24*, 3549−3554.
(30) Hu, P. A.; Li, K.; Chen, W L *J. Microench. Microeng.* **2010**, *7*, 070532.
(31) Wu, L. Li.; Fang, P. X. S.; Zhai, T. Y.; Dai, L.; Liao, M. Y.; Koide, Y.; Wang, H. Q.; Bando, Y.; Golberg, D. *Adv. Mater.* **2010**, *22*, 3161−3165.
(32) Wang, Z. R.; Wang, H.; Liu, B.; Qiu, W. Z.; Zhang, J.; Ran, S. H.; Huang, H. T.; Xu, J.; Han, H. W.; Chen, D.; Shen, G. Z. *ACS Nano* **2011**, *5* (10), 8412−8419.
(33) Hu, P. A.; Zhang, J.; Wen, Z.; Zhang, C. *Nanotechnology* **2011**, *22*, 335502.
(34) Liu, S.; Wei, Z.; Cao, Y.; Gan, L.; Wang, Z. X.; Xu, W.; Guo, X. F.; Zhu, D. B. *Chem. Sci.* **2011**, *2*, 796−802.
(35) Howard, I.; Fischer, A.; Hoogland, S.; Clifford, J.; Klem, E.; Levina, L.; Sargent, E. H. *Nature* **2006**, *442*, 180−183.
(36) Fang, X. S.; Bando, Y.; Liao, M. Y.; Zhai, T. Y.; Gautam, U. K.; Li, L.; Koide, Y.; Golberg, D. *Adv. Funct. Mater.* **2010**, *20*, 500−508.
(37) Li, L.; Fang, X. S.; Zhai, T. Y.; Liao, M. Y.; Gautam, U. K.; Wu, X. C.; Koide, Y.; Bando, Y.; Golberg, D. *Adv. Mater.* **2010**, *22*, 4151−4156.
(38) Zhang, A.; Kim, H. K.; Cheng, J.; Yu, H. *Nano Lett.* **2010**, *10*, 2117−2120.
(39) Blum, V.; Gehrke, R.; Hanke, F.; Havu, P.; Havu, V.; Ren, X.; Reuter, K.; Scheffler, M. *Comput. Phys. Commun.* **2009**, *180*, 2175.
(40) Perdew, J. P.; Burke, K.; Ernzerhof, M. *Phys. Rev. Lett.* **1996**, *77*, 3865.
(41) Perdew, J. P.; Burke, K.; Ernzerhof, M. *Phys. Rev. Lett.* **1997**, *78*, 1396.